

Mechanical properties of material in Q345GJ-C thick steel plates

Na Yang ^{*1}, Chao Su ^{2a}, Xiao-Feng Wang ^{1b} and Fan Bai ^{1c}

¹ Beijing's Key Laboratory of Structural Wind Engineering and Urban Wind Environment,
School of Civil Engineering, Beijing Jiaotong University, Beijing, China, 100044

² Hainanprovince Institute of Architectural Design, Haikou, China, 571199

(Received November 03, 2015, Revised May 01, 2016, Accepted May 08, 2016)

Abstract. Thick steel plate is commonly found with mega steel structures but its properties have not been fully explored. Grade Q345GJ-C steel plate with thickness ranging from 60 mm to 120 mm are studied in this paper. Both the static and cyclic performance of material in different directions (horizontal and through-thickness directions) and locations (outer surface, 1/4 thickness and mid-depth) are experimentally obtained. The accumulative damage during cyclic loading is also calculated by using bilinear mixed hardening (BMH) constitutive relationship together with the Lemaitre's damage model. Results show that the static properties are better at the outer surface of thick steel plates than those at mid-depth. Properties in through-thickness direction are similar to those at mid-depth in the horizontal direction. The cyclic performance at different locations of a given plate is similar within the range of strain amplitude studied. However, when damage parameters identified from monotonic tensile tests are included in the numerical simulation of cyclic loading tests, damage is found accumulating faster at mid-depth than close to outer surface.

Keywords: thick steel plate; mechanical properties; cyclic response; material test; damage evolution; Lemaitre's model

1. Introduction

Structural steel components fabricated from thick steel plates have been popularly used in engineering in recent years. They are commonly used in column bases, fabricated columns and the main trusses. However, brittle fracture has been found in the thick steel plates during welding or in the servicing period. This phenomenon is believed related to the internal defects in plates and the complicated loads they undergo.

During the smelting progress of the steel plate, segregation of material may occur, particularly in thick steel components. Non-metallic inclusions such as sulphur, phosphorus and manganese coalesce towards the center of the thick plate due to uneven cooling and solidification (Radis and Kozeschnik 2010, Hasegawa *et al.* 2001). These inclusions are present in sheets or strips along the direction of rolling and pressing which is perpendicular to the through-thickness direction (Z-

*Corresponding author, Professor, E-mail: nyang@bjtu.edu.cn

^a Master, E-mail: 12121100@bjtu.edu.cn

^b Associate Professor, E-mail: wangxiaof@bjtu.edu.cn

^c Ph.D. Candidate, E-mail: 13115291@bjtu.edu.cn

direction). Therefore, when the plate is under complicated stresses, such as the welding residual stresses, micro cracks and micro voids would initiate along the rolling direction of the sheets and extend to form fissures/cracks (Wang *et al.* 2010, Takashi 2004).

This type of defect reduces the mechanical properties of thick steel plates, especially those in the Z-direction. Researches (Takashi 2004, Kanazawa *et al.* 1976, Kuwamura *et al.* 2003) showed that the higher sulphur content in thick plate, the worse would be the properties in the Z-direction and the easier brittle fracture of the plate would occur. Therefore, sulphur content and the reduction of area of material in the Z-direction in tensile test are the usual engineering measures of lamellar tearing tendency. Wang *et al.* (2011a, b, c) found that the defects also influence the impact toughness and fracture toughness of steel and they proposed a material selection methods based on the toughness indices. However, the fabricated components from thick steel plates are designed mainly to resist large seismic loads in civil engineering structures but existing researches focused more on the static properties and toughness of the thick steel plates with no reference to the cyclic response and damage accumulation during the loading process. A full-scale reversed loading test of steel box-beams has been conducted (Kuwamura *et al.* 2003), but most of the specimens cracked in the first loading cycle. Damage accumulation in steels during cyclic loading was also studied (Su *et al.* 2002, Pironi and Bonora 2003, Zhang and Wu 2011, Li *et al.* 2012, Shi *et al.* 2012, Su *et al.* 2014) with many models developed, but there is not a model proposed for thick steel plates.

The seismic loading scenario corresponds to reverse cyclic loading at the level of material. Considering that full-scale tests for thick steel plates are expensive and difficult to perform (as it needs large reaction force), it is a better way to investigate the mechanical properties of material in the plate with small specimens. In this paper, both the static and cyclic mechanical properties of thick steel plates are investigated based on material tests. Damage evolution during cyclic loading in thick steel plates is also described in terms of the continuum damage mechanics (Lemaitre and Chaboche 1990). Laboratory experiments including standard monotonic tensile and cyclic loading are performed. Test samples are obtained from Grade Q345GJ-C thick steel plates with thickness ranging from 60 mm to 120 mm. The load-displacement curves from the monotonic tensile tests are plotted, and the hardening process is fitted with the Power law hardening curve. The cyclic tests include increasing amplitude (IA) and constant amplitude (CA) strain loading. The skeleton curves are obtained through the IA loading and well fitted with the Ramberg-Osgood model (Ramberg and Osgood 1943). Bilinear mixed hardening constitutive relationship (Hodge 1957) together with the Lemaitre's damage model (Lemaitre 1985) is developed and implemented into ABAQUS. The damage parameters for each group of samples are calibrated according to a proposed criterion with repeated tensile test as well as the monotonic load-displacement curve. Then the damage accumulations in different groups of samples during cyclic loading are calculated and discussed.

2. Experimental study

Laboratory experiments with four different thick steel plates are performed to obtain the mechanical properties of material for further study. The experiments consist of monotonic tensile test, cyclic loading test and repeated tensile test. The main static mechanical properties are obtained through the monotonic tensile tests while two kinds of loading protocols are applied for the cyclic response analysis. Damage parameters are obtained by repeated tensile in latter section.

Table 1 Chemical composition of Q345GJ-C thick plates

	C	Si	Mn	P	S	V	Nb	Al	Cr	Ni	Cu	Ti
60 mm	0.13	0.30	1.30	0.012	0.002	0.004	0.029	0.035	0.02	0.02	0.02	0.016
80 mm	0.15	0.30	1.51	0.012	0.003	0.006	0.022	0.029	0.057	0.03	0.02	0.013
100 mm	0.16	0.31	1.51	0.010	0.002	0.005	0.024	0.031	0.04	0.01	0.02	0.016
120 mm	0.19	0.32	1.46	0.013	0.004	0.001	0.010	0.035	0.03	0.07	0.05	0.005

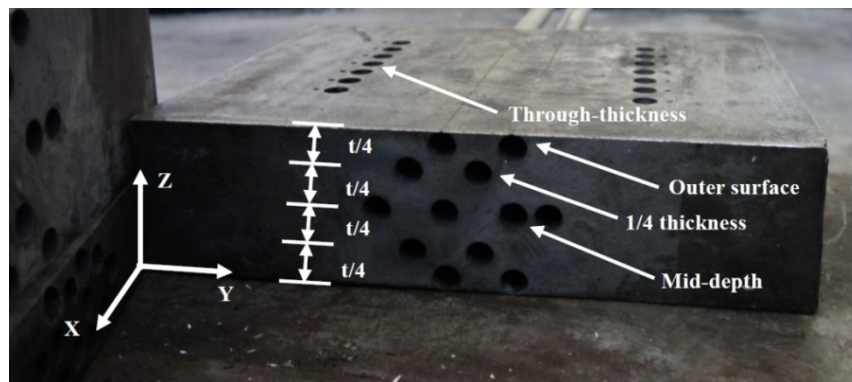


Fig. 1 Specimen locations in thick steel plate

2.1 Preparation for the experiments

Test samples are obtained from steel plates of Grade Q345GJ-C with the thickness of 60 mm, 80 mm, 100 mm and 120 mm. The chemical composition of the parent metal is shown in Table 1. Both properties in the horizontal and Z-direction of the plates are investigated. As shown in Fig. 1, samples are drilled from different positions of the plate and classified in groups according to the position and orientation of sample, e.g., close to the outer surface, 1/4 thickness away from the outer surface, at mid-depth of plate, and in the Z-direction. Whether the horizontal direction is along the rolling direction or not is not known.

There are three specimens for monotonic tensile test, two specimens for cyclic loading test and three specimens for repeated tensile test in one group. The dimension of the specimens as shown in Fig. 2 is according to design standard (SAPRC 2010). The details of the geometry dimension are listed in Table 2. Monotonic tensile specimens in Z-direction are special because of the short length limited by the thickness. Since the standard requires that gage length should be five times the diameter of specimens, the samples in Z-direction are designed to have a smaller cross-section. The overall length for all the horizontal specimens of cyclic loading test is 120 mm and that for the Z-direction specimen is their corresponding thickness. For Z-direction specimen in the 60 mm plate, the designed end section length is too short to grip tightly by the test machine. Therefore, the tests on the cyclic performance in Z-direction of 60 mm thick plate are not arranged. The overall length of horizontal specimen of repeated tensile test is 120 mm and that for the Z-direction specimen is the corresponding thickness of plate. Specimens from Z-direction of 60 mm and 80 mm thick steel plates are not prepared because their lengths are too short to be held firmly by the grips.

Table 2 Geometry details and number of specimens (unit: mm)

Type	Location	D	d	L_c	L_t	R	Number of specimens
Monotonic tensile	Horizontal	14	10	55	145	10	3
	60 mm Z-direction	7	3	18	60	2.5	3
	80 mm Z-direction	7	3	18	80	2.5	3
	100 mm Z-direction	7	3	18	100	2.5	3
	120 mm Z-direction	10	5	30	120	6	3
Cyclic loading	Horizontal	14	7	16	120	16	2
	80 mm Z-direction	14	7	16	80	16	2
	100 mm Z-direction	14	7	16	100	16	2
	120 mm Z-direction	14	7	16	120	16	2
Repeated tensile	Horizontal	14	7	18	120	7.5	3
	100 mm Z-direction	14	7	18	100	7.5	3
	120 mm Z-direction	14	7	18	120	7.5	3

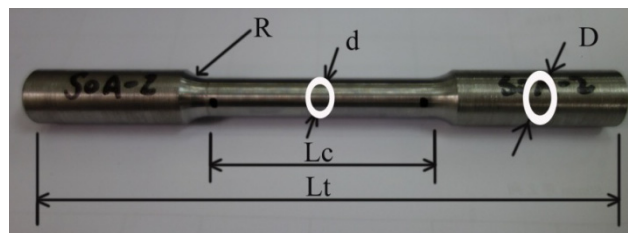


Fig. 2 Geometry dimension of test specimens

The loading equipment is the INSTRON 8801 hydraulic fatigue testing machine. Since the gauge lengths of specimens are different, two extensometers with gauge length of 12.5 mm and 25 mm are used to measure the strain of specimens. The measurement range is ± 5 mm, corresponding to $\pm 40\%$ and $\pm 20\%$ strains according to the different gage lengths. The percentage strain refers to the ratio of axial elongation to the gauge length of the extensometer.

2.2 Loading protocols

Monotonic tensile specimens are conducted according to the standard procedure (SAPRC 2010) with a constant strain rate 0.00033/s until fracture. Cyclic loading patterns are also programmed in a strain control mode. The cyclic loading frequency is 0.1 Hz. Fig. 3 shows the two strain amplitude loading patterns used in testing, namely, increasing amplitude (IA) strain loading and constant amplitude (CA) strain loading. For all strain histories, the IA loading protocol consists of three cycles at each stage of strain reversal, including $\pm 0.4\%$, $\pm 0.8\%$, $\pm 1.2\%$, $\pm 1.6\%$, $\pm 2.0\%$, $\pm 2.4\%$. The specimens are not allowed to fracture during cyclic loading for protecting the extensometer. Therefore, the loop number of CA strain loading is constant. The CA strain loading protocol consists of 30 cycles with the strain reversal at $\pm 1.5\%$. There are two specimens in a group and each specimen is test with one loading pattern. Repeated tensile tests are conducted for

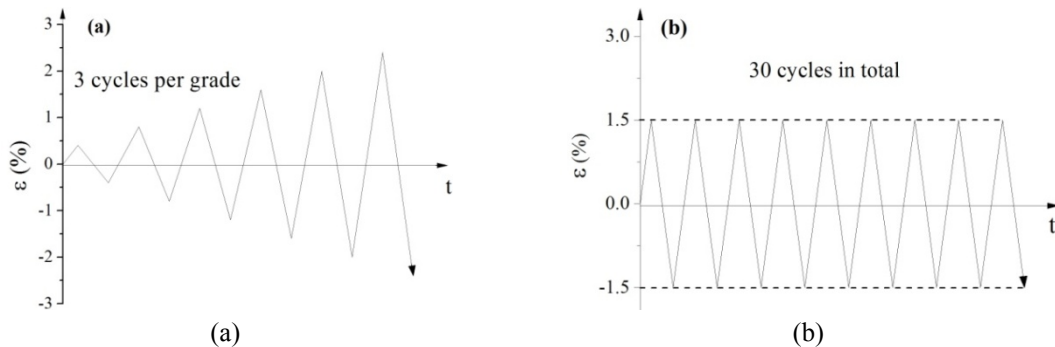


Fig. 3 Cyclic loading protocols (a) increasing amplitude strain loading (IA); (b) constant amplitude strain loading (CA)

identification of parameters in Lemaitre's damage model. Specimens will be unloaded and reloaded during monotonic tensile loading at different strain. Three specimens are prepared for the test in each group to obtain more unloading points. The repeated tensile test will be detailed in latter section.

3. Experimental results and discussions

3.1 Static properties

The yield strength f_y , Young's modulus E , ultimate strength f_u , yield ratio f_y/f_u , reduction of area r_e and elongation e_l after fracture are obtained from the tests. It is noted that the Young's modulus is about 214 GPa for all the specimens.

Standard GB/T 228-2010 (SAPRC 2010) suggests that the mechanical properties at 1/4 thickness of thick plates should be taken to represent the properties of the whole steel plate. Therefore, all properties of the test specimens are normalized by dividing with the corresponding value at 1/4 thickness of the same thick plate. For instance, $f_{y,i}/f_{y,1/4}$ denotes the yield strength of the i_{th} specimen is divided by the mean yield strength at 1/4 thickness. This normalization is applied to all the property indices, including f_y , yield ratio, r_e and e_l , and the scattered diagrams on these indices are plotted in Fig. 4 and compared with the base line at unity.

In Fig. 4(a), the yield strength f_y shows a clear decreasing tendency with the distance away from outer surface. It is probably because the inclusions or chemicals that influence the yield strength coalesce more at 1/4 thickness than at other locations. This observation is noted in all the plates, but the 120 mm thick plate has the weakest material at 1/4 thickness instead. The tendencies for different plates are different but the lowest strength is higher than $0.9 f_{y,1/4}$. Hence, $0.9 f_{y,1/4}$ is recommended as reference strength when thick steel plates are selected for construction. In Fig. 4(b), the ultimate strength f_u shows no obvious pattern but it seems to stay at the same level from outer surface to mid-depth for a given plate (with the largest difference of 5% in the Z-direction) except for the 120 mm thick plate. The yield ratio represents the reserve of safety of material. A low yield ratio suggests a large reserve of stress resistant after yielding. The yield ratio of all the plates shows the same pattern that it decreases with the distance away from the outer surface as shown in Fig. 4(c). This means although the yield strength decreases from the outer surface to mid-depth but the safety reserve improves. Fig. 4(d)-(e) show that r_e and e_l are around the base line

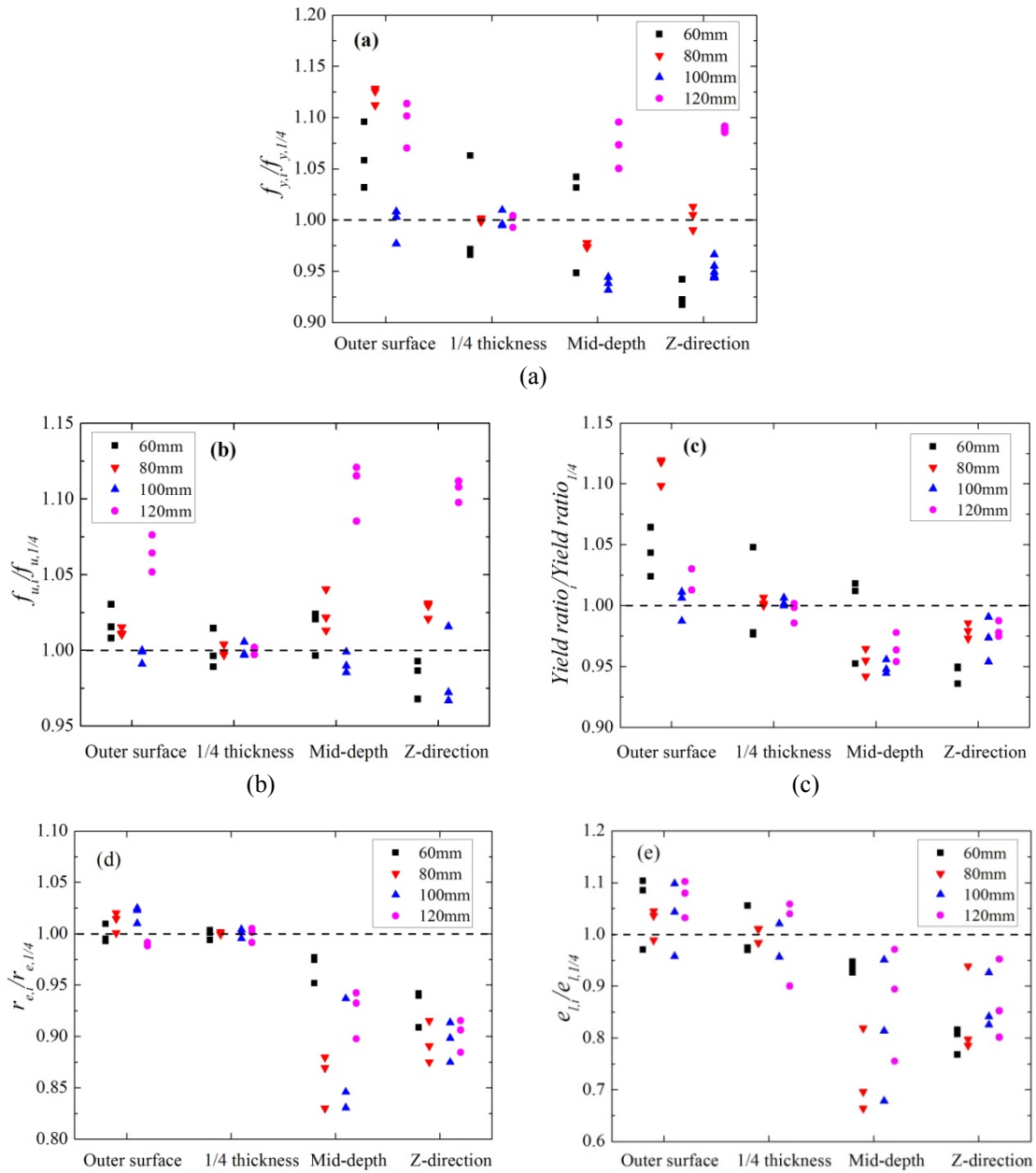


Fig. 4 Scatter diagrams of static property indices; (a) yield strength f_y ; (b) ultimate strength f_u ; (c) yield ratio; (d) reduction of area r_e ; (e) elongation e_l

at the outer surface and 1/4 thickness but they drop rapidly at mid-depth. Since they are ductility indices, this implies that the material tends to be more brittle at mid-depth. Micro-voids and micro-cracks may have developed more quickly at mid-depth than close to the outer surface. Therefore, $0.8r_e$ and $0.6e_l$ are recommended as reference values according to the experimental data for

selection of plate thickness in engineering application.

Properties in Z-direction in Fig. 4 are noted almost below the base line. It is also found that they are similar to that at mid-depth. The material test in standard monotonic tensile tests is within the gage length of the specimen. In fact, the gage length of specimen in Z-direction covers the mid-depth and the 1/4 thickness. If there is no large defect in the Z-direction specimen, properties in Z-direction are influenced mostly by the chemical compositions. Therefore, it is reasonable to expect that the properties in the Z-direction and horizontally at mid-depth are similar.

The property indices provide the reference of static performance of material with the hardening curve describes the whole process in monotonic loading. In material test, the extensometer is removed before large necking of the specimen for protection of the test machine in case of sudden fracture. The true stress-strain relation after the removing of extensometer can be predicted with curve fitting. The Power law hardening function, written in terms of true stress and true strain, is applied for the prediction. The fitted hardening parameters can be introduced as material properties in numerical simulation. The true stress is defined as $\sigma = \sigma_{nom} (1 + \varepsilon_{nom})$ and the true strain is defined as $\varepsilon = \ln (1 + \sigma_{nom})$, where σ_{nom} and ε_{nom} are nominal stress and nominal strain, respectively. The model is written as

$$\sigma = k\varepsilon_p^n \quad (1)$$

Where $\varepsilon_p = \varepsilon - \sigma / E$ is the plastic strain; k and n are the hardening parameters.

The fitted curves are shown in Fig. 5 and the corresponding hardening parameters, k and n , are also indicated in the legends. It is noted that the hardening curves at different locations of plate almost overlap except for the 120 mm thick plate where the curve at mid-depth is the highest of the group and that at 1/4 thickness is the lowest. This observation is the same for f_y and f_u . This shows that the stratification of material is most serious in 120 mm thick plate. It is also found that the fitted curves in Z-direction are close to the ones at mid-depth or 1/4 thickness of the plates, especially for 80 mm and 120 mm thick plates, where stratification of material is more noticeable. This gives another evidence that the mechanical properties of material in the central layer of thick plate are the same in the Z-direction and in the horizontal direction. It is also noted that the curves from 1/4 thickness seem to be the lowest among different locations in the same plate for all the plates studied.

As shown in Fig. 5(e), the hardening curves from 1/4 thickness of these four plates are compared to differentiate the hardening capability of the plates. In order to eliminate the potential variability between different plates, the true stress is normalized with $f_{y,1/4}$ of corresponding thick plate. The hardening capability in 60 mm thick plate is noted the weakest while that in 80mm thick plate is the highest and those in 100 mm and 120 mm thick plates are very similar. The hardening ratio ranges from 1.76 to 1.92 at 16% plastic strain. 16% strain is the upper limit of the measured range of extensometer in monotonic tensile test. There is no obvious pattern observed in the relationship between the hardening capability and plate thickness.

3.2 Cyclic properties

The typical IA cyclic loading experimental curves were shown in Fig. 6, and will be replaced by skeleton curves for clearly discussion. Skeleton curve, known as the envelop curve of strength in cyclic loading, is essential for seismic design of the structural components. The skeleton curves of IA loading specimens are shown in Fig. 7. Since there are three cycles for a particular strain amplitude, each data point in the skeleton curve represents the mean value of the stresses at the

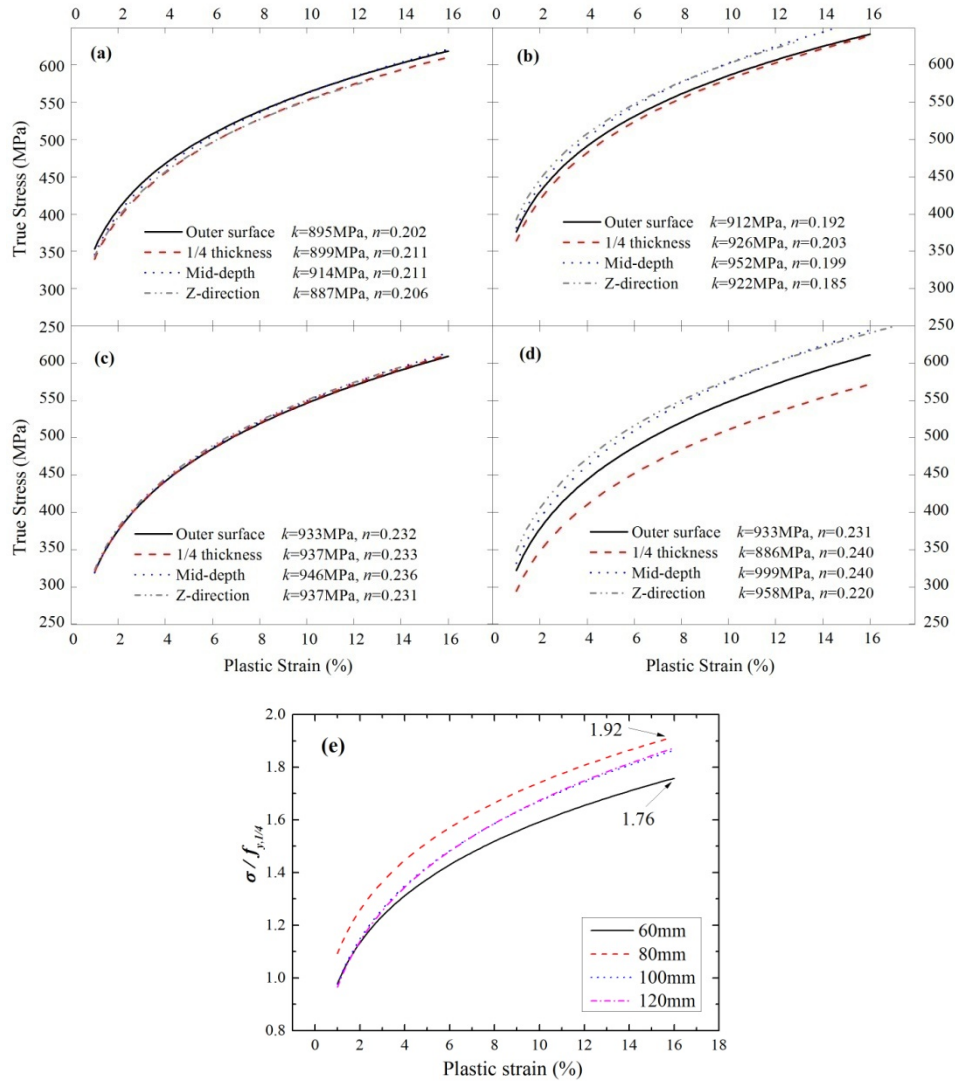


Fig. 5 Fitted curves of specimens (a) 60 mm; (b) 80 mm; (c) 100 mm; (d) 120 mm; (e) hardening curves between thick plates

corresponding strain amplitude from each cycle. It is noted that the skeleton curves from different locations in the same plate almost overlap, and curves from different plates exhibit similar cyclic behaviors. The largest difference exists at 1/4 thickness of 120 mm plate as shown in Fig. 7(d) where the skeleton curve is about 8.9% lower than others. All the skeleton curves show good cyclic hardening behavior. The maximum stresses of the skeleton curve at 2.4% strain have been increased by 30.8%, 25.2%, 14.0%, 34.8% compared with the monotonic curves for the 60 mm, 80 mm, 100 mm, 120 mm thick plates, respectively. Here, 2.4% strain is the upper limit of the measured range of extensometer in the cyclic loading test.

To describe and compare the cyclic hardening responses in different groups more conveniently, the Ramberg-Osgood (RO) model (1943) is applied to fit the skeleton curves. It provides a power

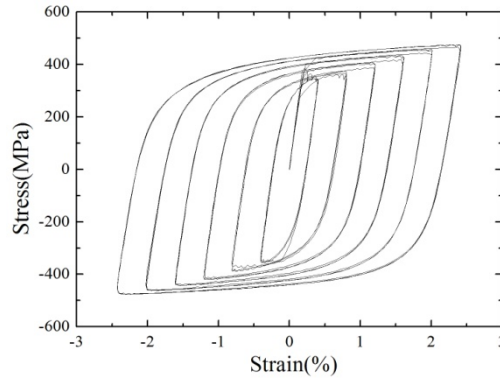


Fig. 6 Typical hysteretic curve of specimens under IA cyclic loading

function of strain amplitude which is related to stress amplitude as

$$\frac{\Delta \varepsilon}{2} = \frac{\Delta \sigma}{2E} + \left(\frac{\Delta \sigma}{2\alpha} \right)^{\frac{1}{m}} \tag{2}$$

where $\Delta \varepsilon$, $\Delta \sigma$ are the strain amplitude and stress amplitude as shown in Fig. 8. α , m are cyclic hardening parameters, respectively. The model gives the strain amplitude values such as $\Delta \varepsilon_1$, $\Delta \varepsilon_2$, $\Delta \varepsilon_3$ when the stress achieving σ_{S1} , σ_{S2} , σ_{S3} at different stress amplitudes of $\Delta \sigma_1$, $\Delta \sigma_2$, $\Delta \sigma_3$.

Since the cyclic hardening capability from different locations in a given plate are approximately the same, only the curves from 1/4 thickness of the plates are selected to be modeled. The RO fitted curves and the corresponding coefficients are shown in Fig. 7(a)-(d). The curves are also normalized in Fig. 7(e) with the yield strength. It should be noted that the cyclic hardening capability of 60 mm thick plate is the weakest while that of 80 mm thick plate is the highest, same as the observations from the monotonic curves. The normalized stress can reach 1.40 and 1.59 $f_{y,1/4}$ at 2.4% strain for 80 mm and 60 mm thick plates respectively.

The cyclic stress-strain curves can be well fitted by the RO model. However, stress is the independent variable and strain is given as a function of stress in this model. It is difficult to transform the model into an expression of stress as a function of strain. Therefore, it is difficult to apply in numerical simulation where a strain value is usually required to initiate the program.

Bilinear hardening model such as isotropic hardening and kinematic hardening are widely used in numerical simulations. As shown in Fig. 8, when $\sigma = \sigma_{S1}$ in monotonic tensile state, the load is reversed until the material reaches another new yielding state. If the new yield stress $|\sigma_{r1}| = |\sigma_{S1}|$, the material is isotropic hardening; if $\sigma_{r1} - \sigma_{S1} = 2\sigma_y$, it is kinematic hardening. In generally, the real cyclic hardening behavior is in between these two cases, which is called bilinear mixed hardening (BMH). If the Mises yield condition is taken into consideration, the mixed hardening function is written as

$$f = \frac{(\sigma_{ij}^{dev} - X_{ij})(\sigma_{ij}^{dev} - X_{ij})}{2} - \frac{1}{3}(\sigma_y + R)^2 \tag{3}$$

where σ_{ij}^{dev} is the deviatoric tensor of stress. X_{ij} is the back stress related to the kinematic hardening. R is the hardening stress related to the isotropic hardening. In Eq. (3), the first item can

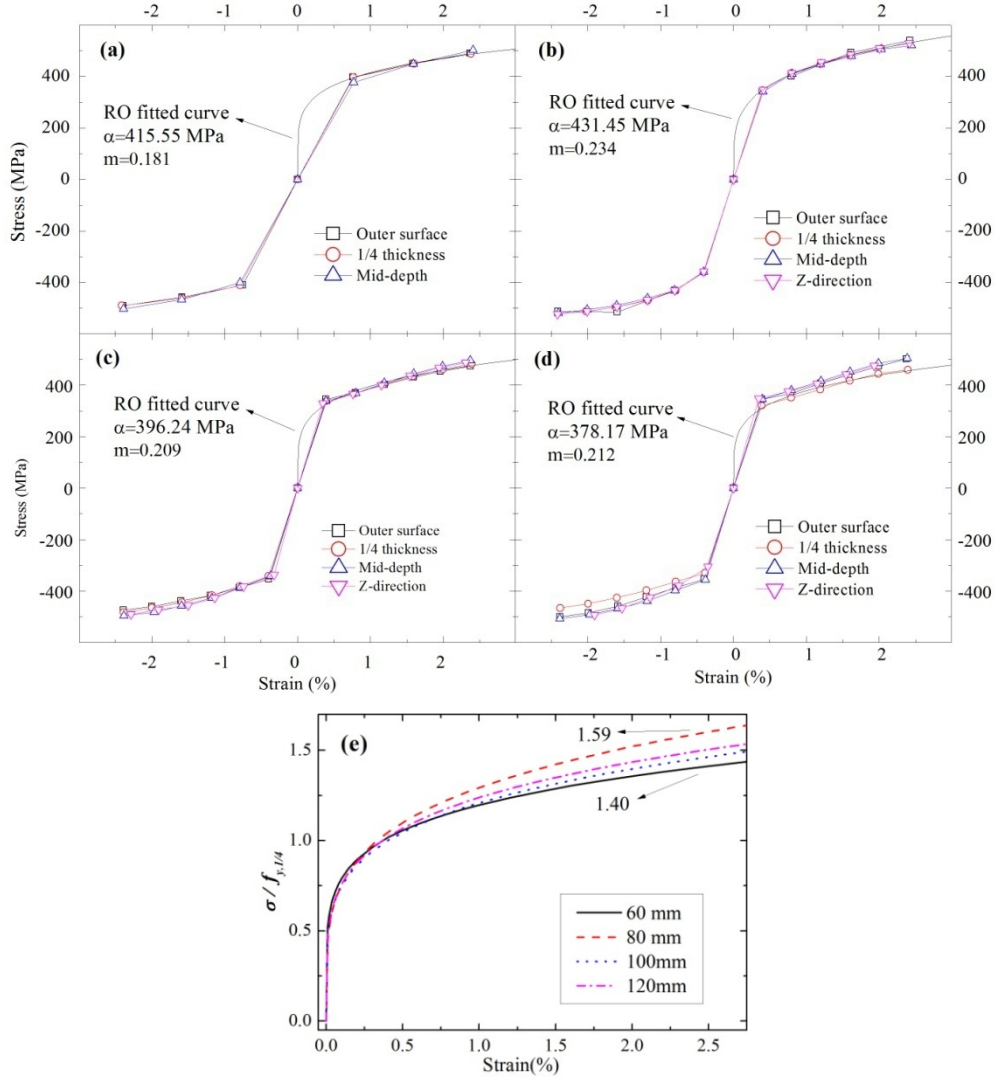


Fig. 7 Skeleton curves of IA loading tests (a) 60 mm; (b) 80 mm; (c) 100 mm; (d) 120 mm; (e) normalized stress

be regard as stresses state, and the second item can be seen as yield surface. According to Prager (1955) and Hodge (1957)

$$\dot{R} = ME_p \dot{p} \tag{4}$$

$$\dot{X}_{ij} = \frac{2}{3}(1 - M)E_p(\sigma_{ij}^{dev} - X_{ij})\dot{\lambda} \tag{5}$$

where $\dot{\lambda}$ is the plastic factor. \dot{p} is the accumulative plastic strain. M is the mixed hardening parameter, ranging from null to unity, where null represents the kinematic hardening and unity represents the isotropic hardening. E_p is the plastic modulus given by

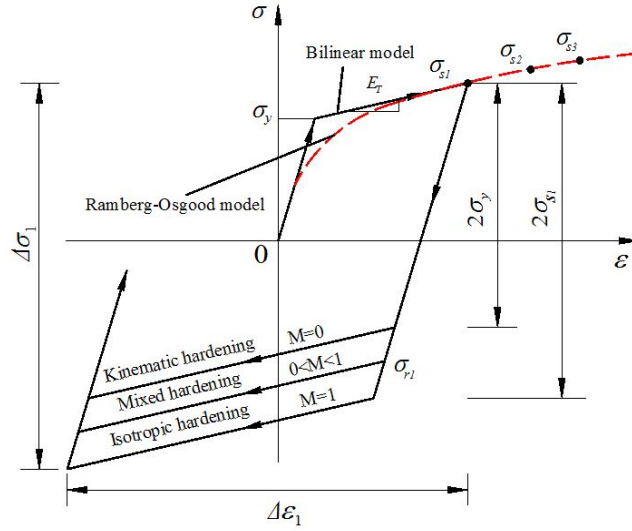


Fig. 8 Ramberg-Osgood model (1943) and the bilinear model (Hodge 1957)

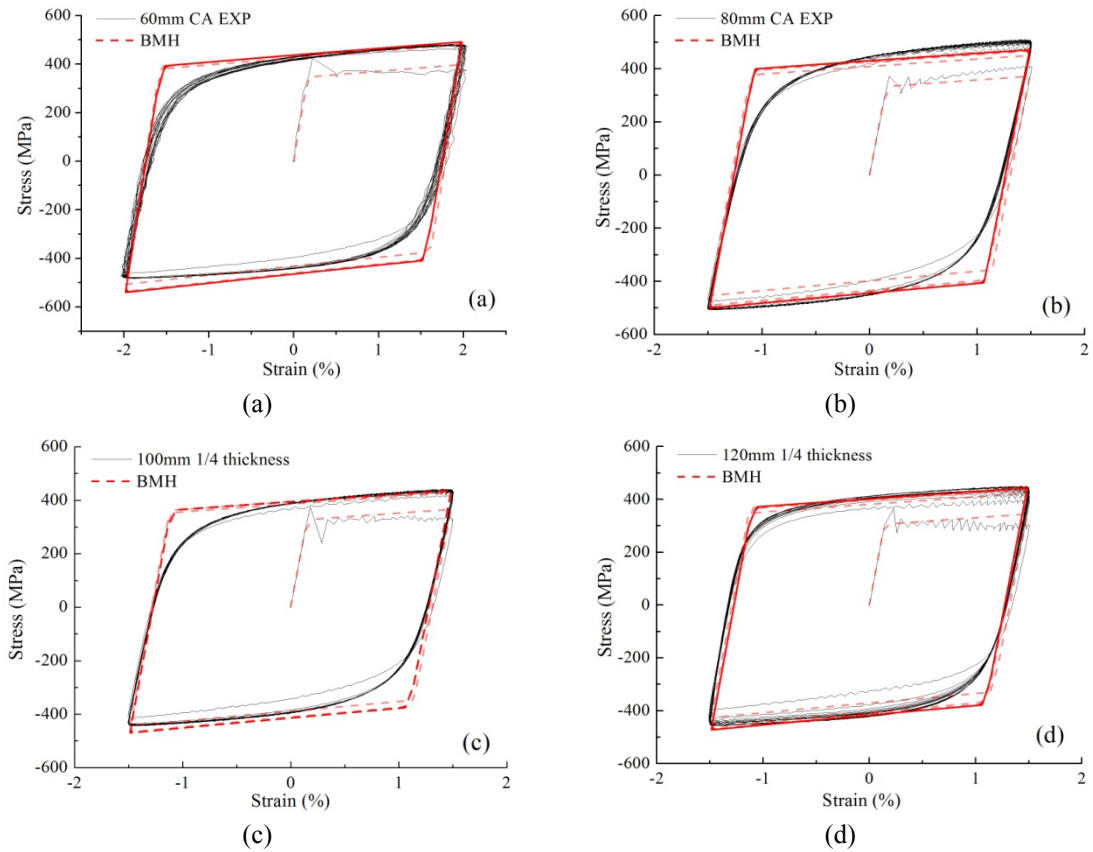


Fig. 9 Comparisons between experimental and BMH curves of CA loading tests; (a) 60 mm; (b) 80 mm; (c) 100 mm; (d) 120 mm

$$E_p = \frac{EE_T}{E - E_T} \quad (6)$$

where E is the Young's modulus. E_T is the tangent modulus constant in the bilinear hardening model.

In the BMH model, the tangent modulus E_T and mixed hardening factor M may change during the cyclic loading. In this paper, E_T is assumed constant since it is difficult to determine E_T in each cycle. M is assumed varying with the plastic strain according to an exponential function as

$$M = M_0 \exp(-\eta \varepsilon_p) \quad (7)$$

where M_0 defines the initiate mixed hardening factor, which is assumed equal to 1.0 in this research. η reflects the rate of change of M .

The cyclic responses of the specimens in CA loading tests do not vary with different locations of thick steel plate as well. The material strength improves much in the first two cycles, and it remains stable in the next cycles. Since the cyclic performance at different locations of a given plate is similar, as shown in Fig. 9, only the specimens at 1/4 thickness of each plate are simulated by employing the BMH model. The numerical stress-strain curves for different groups are compared with the experimental ones. Since there is little difference of cyclic response between the plates, only one set of parameters are compared. Fitting the tangent modulus of the specimens in CA loading, the mean value $E_T = 0.0152E$ is obtained. It is found that when $E_T = 0.0152E$ and $\eta = 30$, the BMH curves agree well with the cyclic response curves of these four plates.

4. Damage estimation

Although the specimens did not fail in cyclic loading tests, damage still accumulates during the loading process. In this paper, Lemaitre's damage model is introduced into the BMH model and the corresponding damage constitutive equations are implemented in ABAQUS. Through numerical simulation, damage evolution in these specimens can be calculated. Before the estimation, damage parameters for different specimens should be obtained.

4.1 Lemaitre's damage model

Damage index D ranges from null to unity, where null represents the virgin material without damage and unity represents the failure of material. Basing on the CDM theory, Lemaitre and Chaboche (Lemaitre and Chaboche 1990, Lemaitre 1985) developed a ductile damage model with the evolution law as

$$\dot{D} = \frac{\sigma_{eq}^2}{2ES(1 - \xi D)^2} R_v \dot{p} \quad \text{if} \quad p \geq p_D \quad (8)$$

where σ_{eq} is Von Mises equivalent stress. ξ is the crack closure parameter, which reflects the micro-crack closure effect in compression. When the material is in compression, cracks and voids tend to shrink, reducing the damage accumulative rate (Lemaitre and Chaboche 1990). S is a damage parameter which should be determined from experiments. p_D is the damage threshold in three-dimensional reference given in Eq. (9). If $p < p_D$, no damage develops

$$P_D = \varepsilon_{PD} \frac{\sigma_u - \sigma_y}{\sigma_{eq} - \sigma_y} \quad (9)$$

where ε_{PD} is the damage threshold in one-dimensional case, which is also determined from experiment. σ_u and σ_y are ultimate stress and yield stress, respectively. R_v is the triaxiality function

$$R_v = \frac{2}{3}(1 + \nu) + 3(1 - 2\nu) \left(\frac{\sigma_m}{\sigma_{eq}} \right)^2 \quad (10)$$

where ν is the Poisson ratio. σ_m is the hydrostatic stress. σ_m / σ_{eq} defines the state of tri-axial stress, which plays an important role in fracture.

The damage model was introduced into the BMH model by assuming the concept of effect stress (Lemaitre and Chaboche 1990)

$$\tilde{\sigma}_{ij} = \sigma_{ij} / (1 - D) \quad (11)$$

where σ_{ij} is the stress tensor. $\tilde{\sigma}_{ij}$ is the effective stress tensor. The Mises yield function is transformed into

$$f = \frac{(\sigma_{ij}^{dev} - X_{ij})(\sigma_{ij}^{dev} - X_{ij})}{2(1 - D)^2} - \frac{1}{3}(\sigma_y + R)^2 \quad (12)$$

According to the orthogonal flow rule, the increment of plastic strain is given by

$$\dot{\varepsilon}_{ij}^p = \frac{\partial f}{\partial \sigma_{ij}} \dot{\lambda} = \frac{\sigma_{ij}^{dev} - X_{ij}(1 - D)}{(1 - D)^2} \dot{\lambda} \quad (13)$$

$$\dot{p} = \sqrt{\frac{2}{3} \dot{\varepsilon}_{ij}^p \dot{\varepsilon}_{ij}^p} = \frac{2}{3} \frac{(\sigma_{ij}^{dev} - X_{ij}(1 - D))_{eq}}{(1 - D)^2} \dot{\lambda} \quad (14)$$

where ε_{ij}^p is the plastic strain tensor. The variable with a dot on top denotes its variation over a small time increment.

The BMH damage model was implemented in ABAQUS via the User defined Material (UMAT) interface. The full details of algorithm for the numerical integration can be found in Su *et al.*'s work (2014). The model will be used to identify the damage parameters and estimate the damage evolution of specimens in cyclic loading tests.

4.2 Identification of damage parameters

The damage parameters S and ε_{PD} in Eqs. (8)-(9) should be determined from experiments. It contains of two steps: identification and calibration. The parameters were identified from repeated tensile tests and calibrated with the experimental load-displacement curves in monotonic tensile tests (Yang *et al.* 2016).

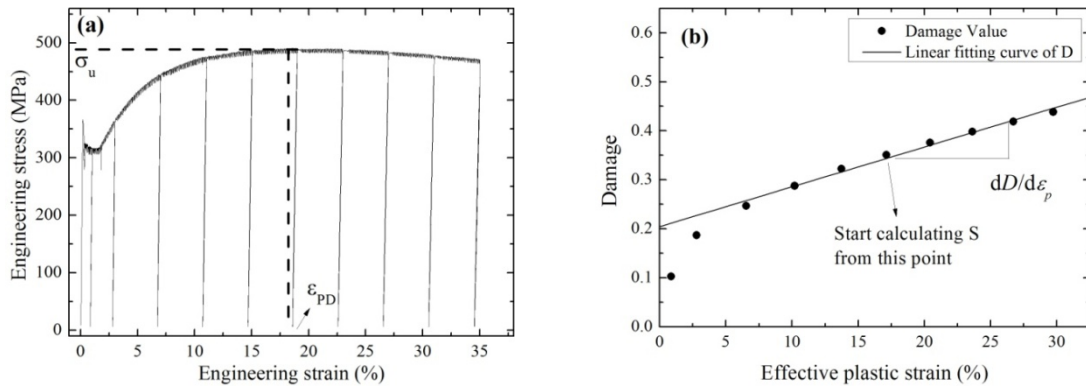


Fig. 10 Identification of damage parameters; (a) stress-strain curve from repeated test; (b) damage evolution sketch

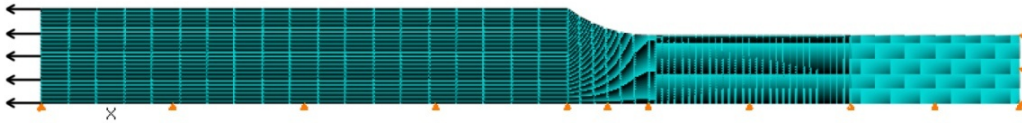


Fig. 11 Axial symmetry model of the specimen

As shown in Fig. 10(a), a series of loading-unloading program is applied on the specimen during the monotonic tensile loading. The damage versus plastic strain relations could be obtained by calculating the degenerated elasticity modulus \tilde{E} at different unloading strain points. Damage is calculated as $D = 1 - \tilde{E}/E$. Subscript i denotes the sequence number of unloading points. Damage in specimens is assumed to initiate after achieving ultimate strength σ_u (Lemaitre 1985), and hardening process without damage is recorded by the extensometer. Therefore, damage threshold ε_{PD} corresponds to the plastic strain on achieving σ_u . Fig. 10(b) shows that the slope of $dD/d\varepsilon_p$ can be linearly fitted to the plastic strain and accumulative damages for calculating parameter S from the following transformed form of Eq. (8)

$$S_i = \frac{\sigma_i^2}{2E_i(1-D_i)^2 \frac{dD}{d\varepsilon_p}} \quad (15)$$

It can be noted that damage increases rapidly in the beginning in Fig. 10(b). Lemaitre and Dufailly (1987) pointed out that instead of damage, this unstable phenomenon is caused by microplasticity and texture development. As a result, the first two data points are ignored, and only the moderately stage was taken for computing the increasing slope. Moreover, damage value in Fig. 10(b) is not correct since the value increased unstable in the beginning. The strain value of the point indicated in Fig. 10(b) is close to damage threshold ε_{PD} . Therefore, S is started calculating from the point. The mean value of parameter S is then obtained.

To validate the identified parameters, the above damage parameters as well as the hardening parameters in Fig. 5, are used as mechanical properties to simulate monotonic tensile tests.

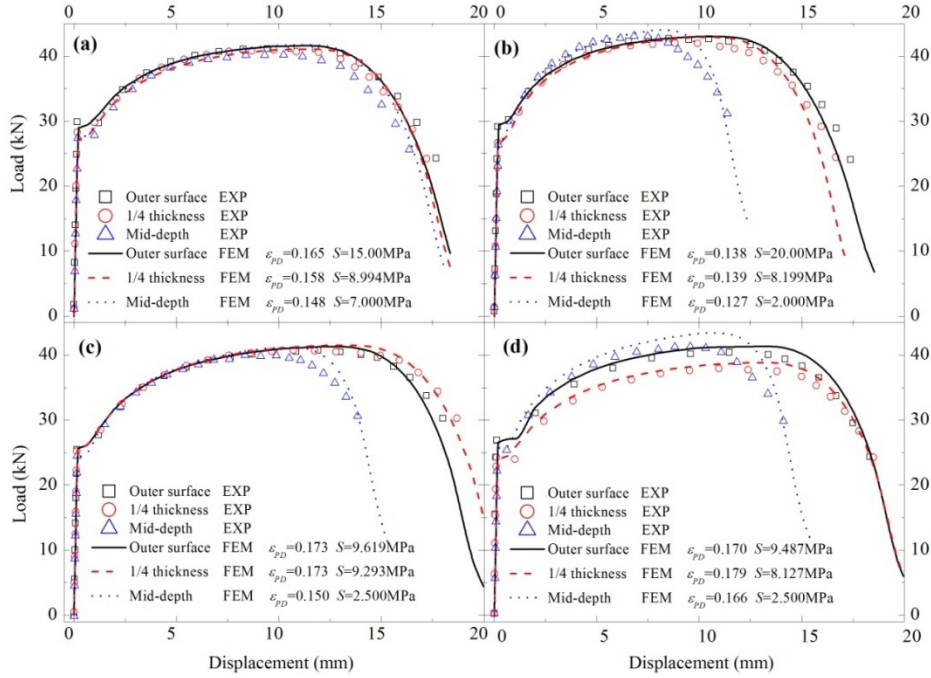


Fig. 12 Comparisons between numerical and experimental curves of monotonic tensile tests; (a) 60 mm; (b) 80 mm; (c) 100 mm; (d) 120 mm

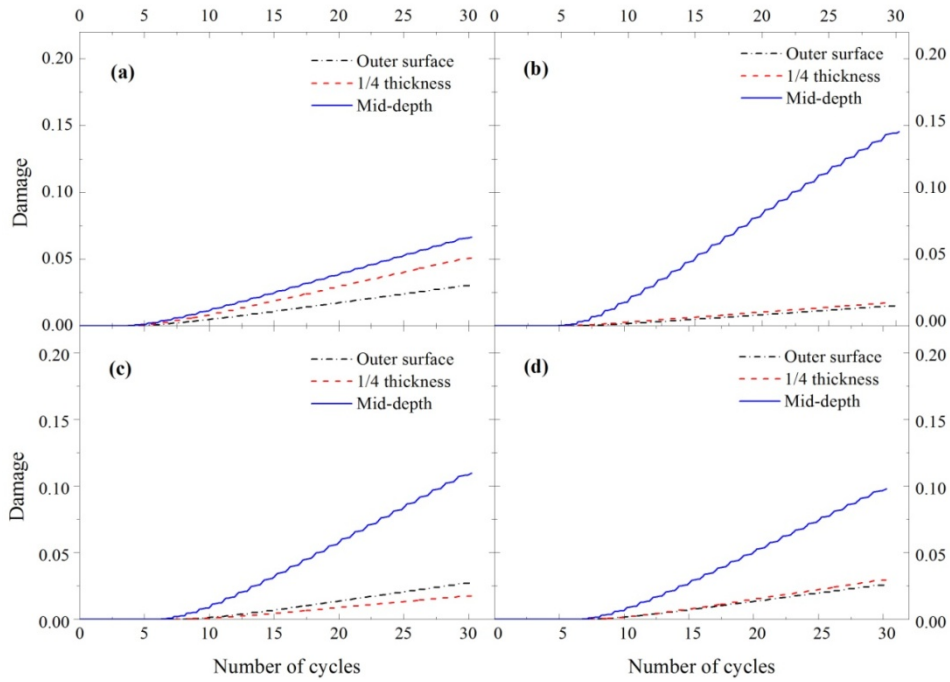


Fig. 13 Damage evolution of CA specimens; (a) 60 mm; (b) 80 mm; (c) 100 mm; (d) 120 mm

An axial-symmetry model of the specimen was built in ABAQUS, with the minimum mesh size 0.1mm in the necking zone (see Fig. 11). Since the brittleness of materials is of concern in structural design, the numerical load-displacement curves are compared with the experimental curves for the weakest specimen in each group. A rule was then made to judge whether the damage parameters are acceptable or not, i.e., *the numerical fracture displacement point is within 5% difference compared with the real fracture point*. Numerical fracture displacement is defined when the numerical load equals to the real fracture load of the weakest specimen. If the difference is larger than 5%, the corresponding parameters, S and ε_{PD} , should be corrected until the rule is met. S defines the rate of damage evolution. A smaller S would lead to faster damage accumulation with sooner fracture occurrence. Damage threshold ε_{PD} defines the plastic strain instant when the damage initiates. A smaller ε_{PD} indicates an early occurrence of fracture. Therefore, the parameters can be adjusted with trial and error in the comparison of numerical and experimental load-displacement curves. The improved damage parameters for different groups of thick steel plates are listed in Fig. 12.

Fig. 12 shows the comparisons between numerical and experimental load-displacement data. The numerical curves are obtained by using the improved damage parameters, and the experimental curves are from the weakest specimen which is the first one fracture in each group. It is noted that the numerical and experimental curves are close to each other for the 60mm thick plate. For the other plates, it is found that specimens close to outer surface show better ductility than those at mid-depth.

4.3 Damage accumulation in cyclic loading

There are two assumptions in the calculation of damage accumulation in Eq. (8): (1) The damage parameters identified from monotonic tensile tests can be used in cyclic loading estimation; (2) crack closure parameter ζ varies with the sign of σ_m / σ_{eq} . ζ equals to 1.0 when it is positive and ζ equals to 0.2 when it is negative (Lemaitre and Chaboche 1990).

The obtained damage threshold ε_{PD} in 4.2 is in one-dimension reference. In essential, the value of ε_{PD} is accumulative plastic strain. The damage will initiate once the accumulative plastic strain meets ε_{PD} , no matter the components under monotonic or cyclic loading. It is also noted that ζ can slow the speed of damage evolution while the material is in pressure, which is closer to actual conditions. Therefore, it is reasonable that the parameter is used from monotonic loading to three-dimension loading.

The number of cycles undergone by the CA specimen is larger than that of IA specimen, so the accumulated damage is more noticeable. Therefore, the damage evolution curves of CA specimens are selected to represent the damage evolution process as shown in Fig. 13. Damage initiates at about the fifth cycle in the 60 mm and 80 mm plates, while it is about the seventh and eighth cycle in the 100 mm and 120 mm thick plates. This can be easily explained that the damage threshold ε_{PD} is larger for the 60 mm and 80 mm plates. It is noted that damage increases with the number of loading cycles. Damage accumulates 60 mm thick plate is slower than in other plates, and damage accumulates faster and larger at mid-depth than that close to outer surface for all the four plates studied.

5. Conclusions

Specimens from four different steel plates of different thickness are test under monotonic tensile and cyclic loading. Both the static performance and cyclic response are discussed. Damage

accumulation during cyclic loading is also analyzed with a proposed strategy. The following conclusions are obtained from the experimental results and data analysis:

- The yield strength, f_y , decreases with increasing plate thickness. Other indices such as the yield ratio f_u , reduction of area of necking e_l and elongation of gauge length r_e show no obvious relation with the thickness. The property indices decrease with the distance away from the outer surface, especially for e_l and r_e except for the ultimate strength f_u . Properties at mid-depth of a given plate are similar to those in the Z-direction.
- Monotonic hardening and cyclic hardening of material at different locations in a given plate are similar. For the four steel plates studied, the monotonic hardening stress ranges from 1.76 to $1.92f_{y,1/4}$ at 16% plastic strain and the cyclic hardening stress ranges from 1.40 and $1.59 f_{y,1/4}$ at 2.4% strain. (16% and 2.4% are the upper limits of the measured ranges of extensometer in monotonic tensile and cyclic loading tests, respectively.) The hardening curves from 1/4 thickness can be used to represent the hardening properties of the corresponding plate.
- Damage parameters of Lemaitre's model are identified with the proposed strategy, and they are introduced into the bilinear mixed hardening constitutive relation for calculating the damage evolution of specimens during the cyclic loading. Damage accumulates faster at mid-depth than close to outer surface.
- The results are limitable since the testing data is only based on one kind of steel plates. However, the paper proposed a method to describe behavior of thick plates under cyclic loading with considering both the cyclic hardening and damage evolution.

Acknowledgments

The research presented in this paper was financially supported by National Natural Science Foundation of China (NSFC-51422801, 51278049, 51078026).

References

- Hasegawa, H., Nakajima, K. and Mizoguchi, S. (2001), "In-situ' observation of phase transformation and MnS precipitation in Fe-Si alloys", *Tetsu-to-Hagane (J. Iron Steel Inst. Jpn.)*, **87**(6), 433-440.
- Hodge, P.G. Jr. (1957), "Discussion on: A new method of analyzing stress and strain in work hardening plastic solids", *J. Appl. Mech.*, **24**, 482-484.
- Kanazawa, S., Yamato, K. and Takashi, I. (1976), "On the assessment of the lamellar tearing susceptibility", *J. Jpn. Weld. Soc.*, **45**(3), 238-244. [In Japanese]
- Kuwamura, H., Iyama, J. and Matsui, K. (2003), "Effects of material toughness and plate thickness on brittle fracture of steel members", *J. Struct. Eng.*, **129**(11), 1475-1483.
- Lemaitre, J. (1985), "A continuous damage mechanics model for ductile fracture", *J. Eng. Mater. Technol.*, **107**(1), 83-89.
- Lemaitre, J. and Chaboche, J.L. (1990), *Mechanics of Solid Materials*, Cambridge University Press.
- Lemaitre, J., and Dufailly, J. (1987), "Damage measurements", *Eng. Frac. Mech.*, **28**(5), 643-661.
- Li, Z.X., Jiang, F.F. and Tang, Y.Q. (2012), "Multi-scale analyses on seismic damage and progressive failure of steel structures", *Finite Elem. Anal. Des.*, **48**(1), 1358-1369.
- Pirondi, A. and Bonora, N. (2003), "Modeling ductile damage under fully reversed cycling", *Comput. Mater. Sci.*, **26**, 129-141.
- Prager, W. (1955), "The theory of plasticity: A survey of recent achievement", *Proceedings of the Institute of Mechanical Engineers*, **169**(1), 41-57.

- Radis, R. and Kozeschnik, E. (2010), "Concurrent precipitation of AlN and VN in microalloyed steel", *Steel Res. Int.*, **81**(8), 681-685.
- Ramberg, W. and Osgood, W.R. (1943), "Description of stress-strain curves by three parameters", *National Advisory Committee for Aeronautics*, Washington, D.C., USA, NACA Technical Note 902.
- Shi, G., Wang, M., Bai, Y., Wang, F., Shi, Y.J. and Wang, Y.Q. (2012), "Experimental and modeling study of high-strength structural steel under cyclic loading", *Eng. Struct.*, **37**, 1-13.
- Standardization Administration of the People's Republic of China (SAPRC) (2010), "Metallic materials - tensile testing - part 1: method of test at room temperature", *GB/T 228.1-2010*, Beijing, China.
- Su, M.Z., Gu, Q. and Guo, B. (2002), "Finite element analysis of steel members under cyclic loading", *Finite Elem. Anal. Des.*, **39**(1), 43-54.
- Su, C., Yang, N., Wang, X.F. and Bai, F. (2014), "A metallic constitutive model considering damage evolution and bilinear mixed hardening", *Proceedings of the 13th International Symposium on Structural Engineering*, Hefei, China, October, pp. 978-985.
- Takashi, I. (2004), "Lamellar tearing (Lecture for practical engineer)", *J. Jpn. Weld. Soc.*, **73**(2), 119-124. [In Japanese]
- Wang, Y.Q., Zhou, H., Shi, Y.J., Chen, H. and Li, S.F. (2010), "A research review on mechanism and prevention of lamellar tearing in thick plate of steel structures", *Prog. Steel Build. Struct.*, **12**(5), 26-34. [In Chinese]
- Wang, Y.Q., Zhou, H., Hu, Z.W., Shi, Y.J. and Chen, H. (2011a), "Experimental analysis of mechanical properties of thick plate in steel structure at low temperature", *J. Civ., Archit. & Environ. Eng.*, **33**(5), 7-12. [In Chinese]
- Wang, Y.Q., Hu, Z.W., Shi, Y.J., Zhou, H. and Chen, H. (2011b), "Study on brittle fracture of thick steel plate based on fracture toughness index (I) ---- classification method", *Low Temp. Archit. Technol.*, **33**(1), 1-4. [In Chinese]
- Wang, Y.Q., Hu, Z.W., Shi, Y.J., Zhou, H. and Chen, H. (2011c), "Study on brittle fracture of thick steel plate based on fracture toughness index (II) ---- selection method", *Low Temp. Archit. Technol.*, **33**(2), 1-4. [In Chinese]
- Yang, N., Su, C., Wang, X.F. and Bai, F. (2016), "Research on damage evolution in thick steel plates", *J. Const. Steel Res.*, **122**(2016), 213-225.
- Zhang, Y. and Wu, Z.Y. (2011), "Mixed hardening constitutive model of steel considering damage evolution", *J. Southeast Univ. (Nat. Sci. Ed.)*, **41**(2), 331-335. [In Chinese]

Notation

The following symbols are used in this paper

D	=	damage variable;
E	=	Young's modulus;
\tilde{E}	=	degraded elasticity modulus;
E_T	=	tangent modulus;
E_P	=	plastic modulus;
e_l	=	elongation at fracture;
f	=	yield function;
f_y	=	yield strength;
f_u	=	ultimate strength;
k, n	=	Power law hardening parameters;
M	=	mixed hardening coefficient;
M_0	=	initial mixed hardening factor;
P	=	accumulated plastic strain;
P_D	=	damage threshold in three-dimensional reference;
R	=	isotropic hardening stress;
R_V	=	triaxiality function;
S	=	damage parameter;
r_e	=	reduction of area at fracture;
X_{ij}	=	kinematic hardening stress tensor;
ν	=	Poisson ratio;
α, m	=	cyclic hardening parameters (Ramberg-Osgood model);
λ	=	plastic factor;
ε	=	strain;
ε_{ij}	=	strain tensor;
ε_p	=	plastic strain
ε_{nom}	=	nominal strain;
ε_{true}	=	true strain;

- $\Delta\varepsilon$ = strain amplitude;
 ε_{PD} = damage threshold in one-dimensional reference;
 σ = stress;
 σ_{nom} = nominal stress;
 σ_{true} = true stress;
 $\Delta\sigma$ = stress amplitude;
 σ_{eq} = Von Mises equivalent stress;
 σ_{ij}^{dev} = deviatoric part of stress tensor;
 σ_{ij} = stress tensor;
 $\tilde{\sigma}_{ij}$ = effect stress tensor;
 σ_m = hydrostatic stress;
 σ_y = yield stress;
 σ_s = cyclic stress for a particular strain amplitude;
 η = exponent variable rate of M ;
 ζ = crack closure parameter.